

A QUANTIFICATION FRAMEWORK FOR POST-LESION NEO-VASCULARIZATION IN RETINAL ANGIOGRAPHY

Sylvain Takerkart ^a, Romain Fenouil ^a, Jérôme Piovano ^b, Alexandre Reynaud ^a,
Louis Hoffart ^{a,c}, Frédéric Chavane ^a, Théodore Papadopoulos ^b, John Conrath ^{a,c}, Guillaume S. Masson ^a

^a CNRS - UMR 6193, Institut de Neurosciences Cognitives de la Méditerranée, Marseille, France

^b INRIA, Team Odysse, Sophia-Antipolis, France

^c Hopital de la Timone, Department of Ophthalmology, Marseille, France

ABSTRACT

We describe an image processing framework designed to detect and quantify the genesis of microscopic choroidal blood vessels. We used fluorescein angiography to monitor the dynamic of neo-vascularization of the retina after inducing lesions with a calibrated laser pulse. The angiogenesis can be revealed by an increase in the overall fluorescence level and/or diffusion size of the lesion. The proposed framework allows measuring both features from mis-aligned angiograms acquired with different gains and contrasts. It consists in aligning all the images, homogeneizing their intensity characteristics and segmenting the lesions. In particular, we implemented a level set segmentation algorithm to delineate the diffusion area. We show that our framework allows detecting neo-vascularization when one of these features changes by less than 10%.

Index Terms— Angiography, detection, registration, segmentation, level sets.

1. INTRODUCTION

Age-related macular degeneration (AMD) is a major disease affecting the retina [1]. The wet form of AMD is characterized by the development of a choroidal neo-vascularization which follows the initial loss of sensitivity of the retinal pigment epithelium. Such proliferation of choroidal neo-vessels results in massive destruction of the retina, further increasing the size of the macular scotomas. Quantitative retinal imaging [2] is therefore critical to follow the evolution of these lesions over time and assess the effects of putative treatments in clinical studies.

This report is part of a larger study investigating the effects of potential drug treatments for reducing angiogenesis following the occurrence of small retinal lesions [3]. Artificial retinal lesions were produced by photocoagulation in anesthetized baboons, using a calibrated laser pulse. We acquired fluorescein angiograms to perform a longitudinal study of the post-lesion neo-vascularization. Choroidal neo-vessels

are both diffuse and microscopic, thus being unresolved with such imaging modality. They however appear on the images as a diffuse area due to leakages in the vasculature tree. Our goal was therefore to develop a quantitative method for delineating and tracking both the diffusion area and the fluorescence level of the lesions. Data were acquired with an angiograph that required manual adjustments of the acquisition parameters (Olympus Medical Systems Corp., Tokyo, Japan; model type GRC-W), thus mimicking many of the variability usually encountered in clinical eye examination. Argentic photos were taken at regular intervals following intravenous injection of fluorescein (10%). Photos were then digitalized offline. Time series covering tens of minutes after fluorescein injections were acquired. For each animal, several dataset were collected before (baseline control), immediately after lesions and up to several weeks after lesions to be able to track the dynamics of retinal neo-vascularisation. Herein, we report the processing framework that was developed to assess these effects in a robust and quantitative way in the perspective of being able to apply it to both experimental (i.e. laser-induced) or clinical (i.e. AMD-like scotomas) studies of macular lesions. After an overview of the full processing flow, we will describe its steps: the contrast adjustment, the registration method and the segmentation algorithm. Finally, we will present our results measured on experimental data.

2. PROCESSING STREAM

Our goal was to design a robust and mostly automated processing stream to analyze sequences of angiograms. Acquiring data for both eyes in the same experimental session implied moving the angiograph before every acquisition, which led to misaligned images with varying contrasts and illumination levels. The proposed framework aims at making all images in a sequence directly comparable, in order to measure the area and fluorescence levels of each lesion. Examples of lesions can be seen on Fig. 3. For an image i and a lesion n , we define the fluorescence index $f(i, n)$ as the ratio of the mean intensity in lesion n over the mean intensity in

the blind spot (or papilla), which we used as a reference region; then, we denote the area by $a(i, n)$. The repositioning of the angiograph introduced some metric distortions between images. To be able to compare measurements of the diffusion area of a lesion across images, we had to correct for these distortions by applying a non-linear registration scheme that would align all images in a sequence. Then, we performed a contrast adjustment based on meaningful image features, to homogenize the intensity characteristics of images throughout the sequence. Finally, we had to identify and delineate each lesion. Considering the complexity of the retinal image content, we decided not to attempt segmenting them from the entire image. Therefore, the operator had to manually select rectangular regions of interests, each containing one lesion. This selection had to be done only once per sequence because the registration was performed previously. The full processing stream for a given input image is described on Fig. 1.

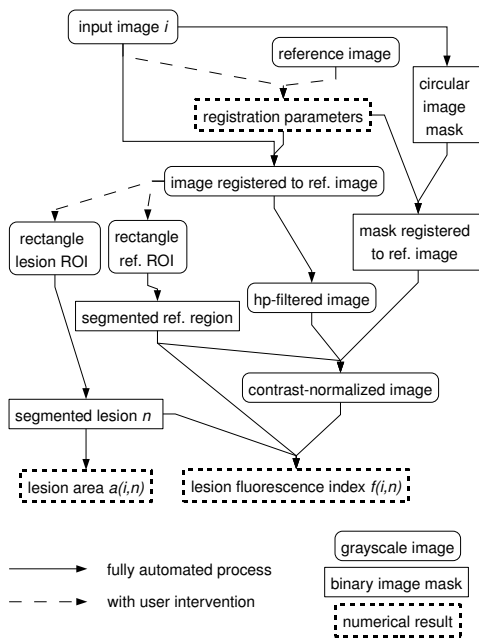


Fig. 1. Description of the full processing stream

3. IMAGE REGISTRATION

The positioning of the angiograph was adjusted manually for almost every image acquisition. Its location is governed by three degrees of freedom: the distance to the target, the height of the apparatus and the rotation around a vertical axis crossing the target position. The observed surface is the eye fundus, which is approximately spherical. Consequently, we used a quadratic model to account for all potential image deformations:

$$\begin{cases} X' = aX^2 + bY^2 + cXY + dX + eY + f \\ Y' = gX^2 + hY^2 + iXY + jX + kY + l \end{cases},$$

where (X, Y) and (X', Y') are the coordinates in the input and reference images, and $(a, b, c, d, e, f, g, h, i, j, k, l)$ are the twelve parameters to be estimated.

We implemented a semi-automatic approach in which the experimenter selects nine (or more) matching points on each image. The choice of these points is facilitated by some automatic pre-processing of the images (filtering, thresholding, vasculature skeletonization, point selection limited to vessels crossings on the skeleton). The parameters are then computed by solving the corresponding linear equations system, which has twelve unknown parameters and eighteen (nine points time two) equations, with a least-square estimator. An example of results produced by our registration algorithm is presented on Fig. 2.

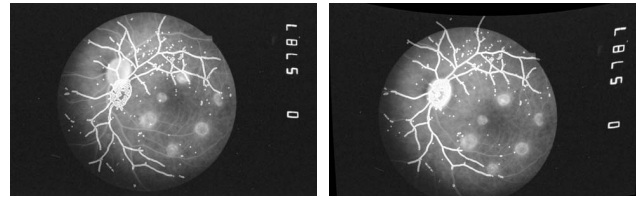


Fig. 2. Registration. The ref. image skeleton overlapped on the original input image (left) and on the registered input image (right)

4. CONTENT-BASED CONTRAST NORMALIZATION

The manual positioning of the angiograph led to large variations in the intensity characteristics of the images. First, the incidence angle can result in low-frequency spatial background variations within an image (as illustrated in the top-right image of Fig. 3), which adds on top of the structural low-frequency spatial variations (presence of the fovea). We therefore applied a high-pass filter on all images to reduce the amplitude of these low-frequency variations.

The average illumination and the dynamic range also showed large variations across images. In order to increase their homogeneity, we performed a contrast normalization by the way of an affine intensity transform that matched two image features across the entire sequence. The first feature is the mean intensity in the reference region - the papilla - which has a similar shape as the lesions, allowing us to use the same segmentation algorithm to extract it automatically. The second image feature to be matched is the mean intensity level within the informative part of the image, which is a circular mask created by the diaphragm of the angiograph. We thus

implemented an automatic detection of this circular mask, that consisted in a filtering, an automatic histogram-based thresholding, followed by a Hough transform.

These two operations produced images with fairly similar characteristics, as illustrated on Fig. 3.

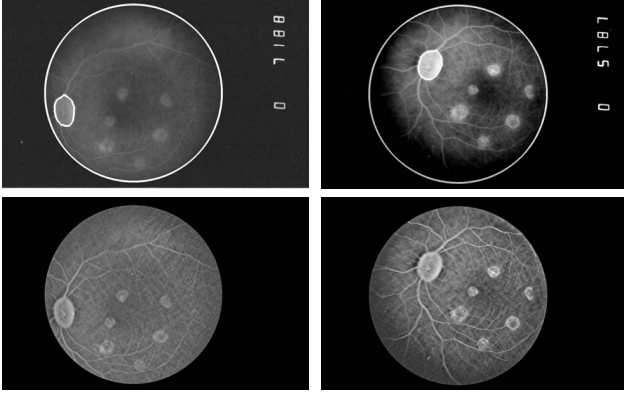


Fig. 3. Contrast normalization. Top row: two images as originally acquired (overlapped are the edges of the circular mask and of the segmented papilla). Bottom row: after filtering and normalization.

5. SEGMENTATION

To extract the lesion (and the papilla) within each rectangular region of interest, we designed a segmentation method that we thought would overcome the three following difficulties: 1. the smoothness of the edges of the lesion; 2. the low frequency drift present in the background; 3. the large blood vessels that can cross the lesion. We chose the active contour model [4], that consists in adjusting an initial closed curve until it fits the border of the region. Our algorithm is based on the level set method [5]: the curve is seen as the zero level of a higher dimensional function, and the motion of the curve is guided by minimizing an energy function which defines the problem. In our case, the energy is composed of two terms: a “data attachment” term and a “shape prior”.

Segmentation models based on locally stopping the contour on high image gradient [6] are not adapted in our case, due to the smoothness of the regions border. This would result in “leaks”, where the lesion borders are too diffuse. Furthermore, the low frequency variations in the image background are not totally eliminated by the high pass filter (Section 4), which prevents using methods based on global statistics. However as can be seen in Fig. 4, these lesions are locally brighter than the background, thus implying different local statistics inside and outside the lesion. Therefore, we decided to use the local Gaussian model [7], which consists in separating two regions modeled by local Gaussian statis-

tics. It is defined by the following energy function:

$$E = \sum_{i \in \{in, out\}} \int_{\Omega_i} -\log p_i(I(x), \Omega_i) dx \quad , \quad (1)$$

with

$$-\log p_i(I(x), \Omega_i) = \frac{(I(x) - \mu_i(x))^2}{2\sigma_i(x)^2} + \frac{1}{2} \log(2\pi\sigma_i^2) \quad , \quad (2)$$

where p_i is the probability for the point x with intensity $I(x)$ to belong to the local region characterized by local mean $\mu_i(x)$ and local variance $\sigma_i(x)$. The evolution equation is obtained by differentiating Eq. (1) as follows:

$$C_t(x) = \frac{(I(x) - \mu_{in}(x))^2}{2\sigma_{in}(x)^2} - \frac{(I(x) - \mu_{out}(x))^2}{2\sigma_{out}(x)^2} + \log \frac{\sigma_{in}^2}{\sigma_{out}^2} \quad ,$$

where μ_{in} , σ_{in} and μ_{out} , σ_{out} are respectively the mean and variance inside and outside the active contour. These local statistics need to be recomputed at each iteration during the curve adjustment.

In some cases, one or several vessels can cross the lesion. Because their intensity is usually close to the one of the lesion, the contour might be attracted by the vessels. Increasing the regularization cannot help preventing this kind of attraction, as these vessels can be large. To overcome this problem, we added in our model a circular shape prior that penalizes the points that are far from the centroid, thus avoiding the contour from being attracted by vessels (see Fig. 4). The prior is defined by the following energy function:

$$E = \int_{\Omega_{in}} -\log p_i(x, \Omega_i) dx + \nu|C| \quad , \quad (3)$$

with

$$-\log p_i(x, \Omega_{in}) = \frac{(x - c_{in})^2}{2\sigma_{in}^2} + \frac{1}{2} \log(2\pi\sigma_{in}^2) \quad , \quad (4)$$

where c_{in} is the centroid of the region, σ_{in} a spatial variance of the region and $\nu|C|$ is a regularization term corresponding to the minimization of the contour length.

In our experiments, this model behaved quite well. It seems to be the most adapted to our case by being robust to both inhomogeneities and soft region edges.

6. RESULTS AND DISCUSSION

To estimate the robustness of the proposed framework, we performed a reproducibility analysis, based on the hypothesis that the measured lesion area and fluorescence index should be identical if measured on angiograms acquired under the same conditions. However, because the fluorescein continuously spreads through the vascular system after its injection and because the lesion itself can evolve between successive

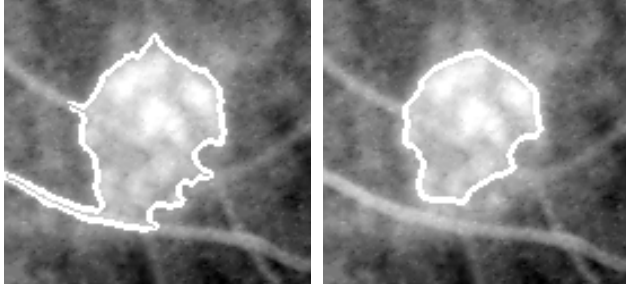


Fig. 4. Segmentation. On the left, without the shape prior, the contour is attracted by the vessel crossing the lesion. On the right, with the shape prior, the segmentation is correct.

experimental sessions (which are separated by ten to fifteen days), it is quasi-impossible to identically reproduce such acquisition conditions. Therefore, we pooled together all images acquired in time bins of one minute (excepted the first minute), separately for each experimental session, thus creating several groups of images G_1, \dots, G_P within each of which we assumed stationarity. Each group gave a sequence of images that was fully analyzed with our processing stream. We then computed the following ratios for each group G_p and each lesion n :

$$F_{G_p}(n) = \frac{\text{std}_{i \in G_p}(f(i, n))}{\text{m}_{i \in G_p}(f(i, n))} \quad \text{and} \quad A_{G_p}(n) = \frac{\text{std}_{i \in G_p}(a(i, n))}{\text{m}_{i \in G_p}(a(i, n))},$$

where $\text{m}(\cdot)$ and $\text{std}(\cdot)$ designate the mean and standard deviations. The normalization of the standard deviation by the mean in the above equations permits gathering results from lesions of different sizes. A weighted averages across all groups is then computed as a measurement of the robustness for the full framework:

$$F = \frac{\sum_p |G_p| \text{m}_n(F_{G_p}(n))}{\sum_p |G_p|} \quad \text{and} \quad A = \frac{\sum_p |G_p| \text{m}_n(A_{G_p}(n))}{\sum_p |G_p|},$$

where $|\cdot|$ is the cardinal of the group.

Using our currently available database, which contains forty usable images with six lesions per image, plus the papilla (which we included in this performance evaluation), we measured $A = 4.80\%$ and $F = 3.67\%$. Assuming a normal distribution for the measured features, the detection power of our method can then be formulated as follows: the neo-vascularization in a lesion will be detected (with a 95% confidence level) if it leads to a variation of the diffusion area by $2A = 9.60\%$ or of the fluorescence index by $2F = 7.34\%$. One can argue that these numbers are over estimated because the aforementioned pooling procedure into time bins introduces a source of variability that is not accounted for in the calculation. Furthermore, the database available to us contained numerous images of bad to average quality. Although

we discarded the worst ones, we do believe that the accuracy of this framework will greatly improve with a more controlled acquisition procedure.

7. CONCLUSION

We described an integrated and mostly automated image processing framework designed to detect and quantify post-lesion retinal angiogenesis. We evaluated its robustness with a reproducibility analysis performed on a database composed of real fluorescein angiograms, and showed that its accuracy allows detecting changes in the diffusion area or the fluorescence level of less than 10%. This framework, that was here tested on artificial laser-induced lesions, also has a direct applications in clinical and pharmacological studies, to follow the evolution of retinopathies or evaluate the effectiveness of a drug to reduce the angiogenesis.

8. REFERENCES

- [1] S. L. Fine, J. W. Berger, M. G. Maguire, and A. C. Ho, "Age-related macular degeneration," *New England Journal of Medicine*, vol. 342, pp. 483–492, 2000.
- [2] N. Patton, T. M. Aslam, T. MacGillivray, I. J. Deary, B. Dhillon, R. H. Eikelboom, K. Yogesana, and I. J. Constable, "Retinal image analysis: Concepts, applications and potential," *Progress in Retinal and Eye Research*, vol. 25, pp. 99–127, 2006.
- [3] R. F. Gariano and T. W. Gardner, "Retinal angiogenesis in development and disease," *Nature*, vol. 438, pp. 960–966, 2005.
- [4] M. Kass, A. Witkin, and D. Terzopoulos, "Snakes: Active contour models," *The International Journal of Computer Vision*, vol. 1, no. 4, pp. 321–331, 1987.
- [5] J. A. Sethian, *Level Set Methods and Fast Marching Methods: Evolving Interfaces in Computational Geometry, Fluid Mechanics, Computer Vision, and Materials Sciences*, Cambridge Monograph on Applied and Computational Mathematics. Cambridge University Press, 1999.
- [6] V. Caselles, R. Kimmel, and G. Sapiro, "Geodesic active contours," Tech. Rep., HP Labs, Sept. 1994, A shorter version appeared at 5th ICCV'95 - Boston.
- [7] J. Piovano, M. Rousson, and T. Papadopoulos, "Efficient segmentation of piecewise smooth images," in *Proc. International Conference on Scale Space and Variational Methods in Computer Vision*, 2007.